Frontiers in Scientific Research and Technology

Online ISSN: 2682-2970
Print ISSN: 2682-2962
http://fsrt.journals.ekb.eg

FSRT J 8 (2024) 1 - 14 10.21608/FSRT.2023.236816.1107

Geology and mineralogy of fluorite-bearing quartz veins hosted by the Late Neoproterozoic syenogranite, south Wadi El Barrah area, south Sinai, Egypt.

Ismail, A. El Akeed*, Hassan, M. Sherif, Mahmoud, M. Gabr

Nuclear Materials Authority, P.O. Box – 530 El Maadi, Cairo, Egypt.

ARTICLE INFO

Article history:
Received 16 September 2023
Received in revised form 21 October 2023
Accepted 24 October 2023
Available online 29 October 2023

Keywords
Uraninite,
Radioactivity,
Fluorite,
Quartz veins,
South Sinai

ABSTRACT

Although uraninite is recorded in the granite pegmatite of south Sinai, this study represents the first record of uraninite in fluorite–bearing quartz veins in south Wadi El-Barrah area, south Sinai. Wadi El-Barrah is a tributary of the famous Wadi Akhdar which can be accessed through the asphaltic road reached to Saint Katherine city. The area is covered with older granites, monzogranite, quartz syenite, pre-syenogranite dykes, syenogranite and post-syenogranite dykes. The area is affected by numerous strike-slip faults and related fractures with NNE-SSW, NW-SE and NE-SW directions. The NNE-SSW and NE-SW fractures are filled with fluorite-bearing quartz veins where some of them show high radioactive intensities. The radiometric study that carried out on these fractures and the associated fluorite–bearing quartz veins indicates that eU ranges from 370 to 780 ppm while eTh ranges from340 to 810 ppm. This abnormal radioactivity is attributed to the presence of uraninite, uranosphaerite and thorutite minerals. Uraninite is of hydrothermal origin as indicated by the presence of galina and deep violet fluorite while uranosphaerite is an alteration product of the uraninite.

1. Introduction

The Neoproterozoic rocks are those having an age ranges between1 billion to 538.8 million years (Stratigraphic Chart 2022). The Neoproterozoic rocks of south Sinai constitute the northern part of the Arabo-Nubian Shield. Granitic rocks in Arabian–Nubian Shield include syn- to late-orogenic granitoids and post-orogenic to anorogenic granitoids, previously identified as older granitoids and younger granitoids, respectively (Bentor 1985). This Shield consists of several lithostratigraphic units affected by metamorphic events and plutonic intrusions in several cycles which took place from Ca. 1100 to 540 Ma. The southern part of Sinai Peninsula is considered as the far most northern part of Arabo-Nubian Shield. It is covered with suits of metamorphic as well as igneous rocks. South Wadi El-Barrah area is located to the north of the well-known Wadi Akhdar south Sinai, Egypt. The area is covered with Precambrian basement rocks that are mainly represented by older granites, monzogranite, quartz syenite, pre-syenogranite dykes, syenogranite and post-syenogranite dykes. These rock suits are invaded by several basic as well as acidic dykes that trend on NE-SW, N-S and NW-SE directions. The area is also affected by numerous strike-slip faults and their related fractures. These faults and fractures are striking mainly on the NW-SE and NE-SW directions.

* Corresponding author at Nuclear Materials Authority
E-mail addresses: elakeed68@gmail.com (Ismail El Akeed)

A spectrometric study is carried out on these fractures to show the distribution of the readio elements indicates the presence of abnormal radioactivity observed along some of these fractures especially those trending on NE-SW and NW-SE directions. The detailed geologic studies of the area show that some of these fractures are filled with quartz and fluorite to form fluorite-bearing quartz veins. The careful examination of these veins indicates the presence of primary uranium mineral Uraninite, Th & U-bearing mineral Thorutite, U & Bi-bearing mineral Uranosphaerite as well as quartz and fluorite.

Although uraninite is recorded in the granite pegmatite of south Sinai (Sherif, 2003 and Bishr et al., 2009), it is not recorded in veins. This study is considered as the first record of uraninite in the fluorite –bearing quartz veins in south Sinai.

The aim of this paper is to study the geology of the area, the radioelements distribution along these veins, the mineralogy of the present minerals and their geneses.

2. Methodology

In order to study the geology of the area, a geologic map was constructed using landsate image obtained from Google Earth where field checking is made to get the accurate field relation between the exposed rock units.

For studying the distribution of ^{40}K%, eU and eTh in south Wadi El Barrah area, a grid pattern was constructed on N-S direction that runs perpendicular on the strike of the zone containing numerous anomalous quartz veins. A total of 132 stations were conducted along twelve equally-spaced profiles where the in-between space of each two

successive profiles is 15 m with station intervals along any profile is 20m. The intensity of radioactivity of every station is measured using the multichannel spectrometer model Gs-512 manufactured by Geofyzika Brno-Czech Republic. It measures the gamma rays as total radiation counts (Tc), equivalent uranium (eU ppm), equivalent thorium (eTh ppm) and ^{40}K%.

Five representative samples were collected from the anomalous veins to identify their U and / or Th-bearing minerals as well as other minerals. The selected samples are crushed using the jaw crushers and sieved using (60-30 mesh) sieves. The sieved samples are subjected to heavy liquid separation using bromoform (specific gravity = 2.82gm/cm3) and methylene iodide (specific gravity = 3.325gm/cm3) and magnetic fractionation using a Frantz Isodynamic Magnetic Separator (Model L-1). The obtained fractions were carefully handpicked using the Binocular Stereomicroscope. The handpicked grains are examined at the laboratory of the Nuclear Materials Authority (NMA) using X-ray diffraction technique and Environmental Scanning Electron Microscope (ESEM). A Phillips X-ray diffractometer (Model PW-1010) with a scintillation counter (Model PW25623/00) and Ni filter. ESEM supported by energy dispersive spectrometer (EDS) unit (model Philips XL 30 ESEM).

3. Geologic background

The studied south wadi El Barah area is covered with a suite of igneous rocks (Fig.1) which are chronologically arranged based on their field relationships, beginning with the oldest as follows:

Older granites are mainly represented by granodiorite. They are corresponding to the older granites defined by Akaad and El- Ramly (1960) and Akaad and Noweir (1980). They also described as subduction-related granites (G1) by Hussein et al. (1982). The granodiorite is considered as the oldest rock unit in the studied area and is exposed on both eastern and southern parts of the mapped area (Fig.1) and contain gabbroic xenoliths of variable sizes and shapes (Fig.2). These older granites are distinguished as orogenic I-type, subduction related granites originated from calc-alkaline magma that emplaced within volcanic-arc tectonic environment (Sherif,1993 and Ibrahim and Khalifa,2004).

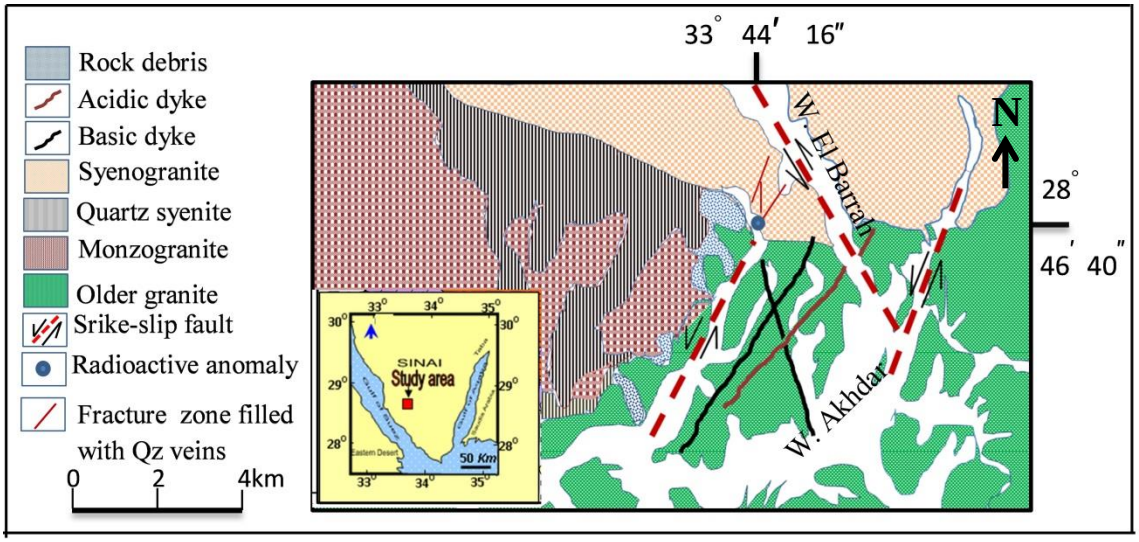

Fig. (1): Geologic map of south Wadi El Barrah area, south Sinai, Egypt.

The younger granites of the studied area can be classified into two phases corresponding to phase (II) and phase (III) younger granites of Sabet et al (1976), Akaad et al (1979) and Abu El- leil (1980). These two phases are monzogranite and syenogranite (El-Sheshtawy,1984; El-Gammal,1986; Habeeb,1989; Sherif,1993; El Galy,1994; Hussein et al. 1999; El- Syed et al. 2004 and Sherif et al. 2022), The monzogranite is mostly exposed at the western side of the mapped area and sharply intruded with both the quartz syenite (Fig.3) and the syenogranite.

The quartz syenite has limited exposure and is only outcropped as small elongated strip on Farsh Zubeir that located on the north western part of the studied area (Fig.1) and sharply intruded by the syenogranite (Fig.4). The syenogranite represents the late magmatic intrusion in the area and outcropped as jointed, fractured, high relief mountainous area with conspicuous red and rosy colours, at the northern part of the study area. They marked with their intrusive sharp with the quartz syenite (Fig.4). Also, some pegmatite pockets (Fig.5) are observed along their contacts with the surrounding rock units i.e. the older granites and the quartz syenite. The studied syenogranite are sometimes containing partly assimilated porphyritic rhyodacite xenolithes (Fig.6) to indicate their later age. The syenogranite is previously defined as muscovite- biotite granite (Sherif, 1993).

The studied younger granites (monzogranite and the syenogranite) are classified as anorogenic A-type granites originated from peraluminous magma that emplaced in

within – plate tectonic environment. (Sherif, 1993and Ibrahim and Khalifa, 2004).

Based on their major and trace elements geochemistry, the studied Gabal Hamra younger granites, north side of the study area, are generally similar to the low Ca granite and equivalent to the group III of the Egyptian Younger Granites (Hussein et al, 1999).

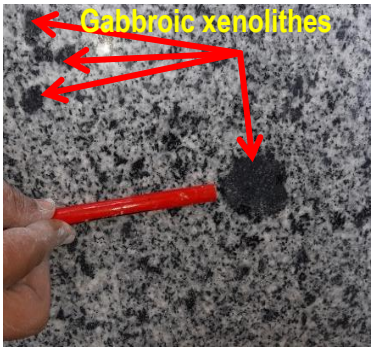

Fig. (2): Gabbroic xenolith with different shapes and volumes within the older granite.

Fig. (3): Sharp contact between the the quartz-syenite and monzogranite.

Fig. (4): Sharp contact between the quartz-syenite and syenogranite.

Dykes are numerous and varied in both their compositions and directions. They can be classified, based on their field relationships with the exposed rock units, into pre- and post syenogranite dyke groups (Fig.7). Both of the two groups are mainly represented by acidic and basic rocks.

The basic dykes are mainly of basaltic composition while the acidic dykes are mostly rhyolite (Sherif, 1993 and Abd EL Azeem,2019). The authors (op cit) concluded that these dykes are dominantly striking in NW-SE and NE-SW. The latter group of dykes is probably corresponding to the post-granite dykes of Akaad and El Ramly (1960).

Fig. (5): Pegmatite pockets along the syenogranite contact with the host rocks.

Fig.(6): Partly assimilated rhyodacite xenolith within the syenogranite.

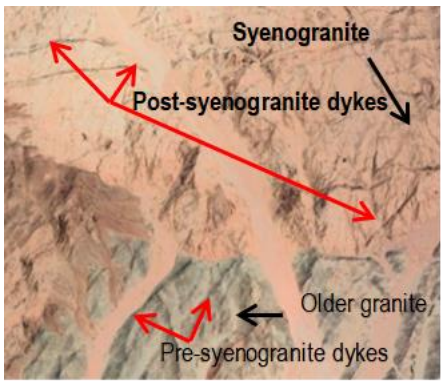

Fig. (7): Pre-, and post- syenogranite dyke groups.

3.1. Geology of the anomalous area

Figure (8) shows the anomalies –bearing syenogranite area (450m x 360m). This area is dissected by parallel set of NNE-SSW and NE-SW striking quartz veins (Fig.8) with 10m width and about 200m length. The syenogranite

around these veins is highly altred with hematitization, silicification and kaolinization appeared as an alteration products (Fig.9). The whole area is affected by numerous fractures with different lengths and trends. The strikes of these fractures are measured and tabulated (Table.1). A rose diagram is made for the measured fractures to diagnosing the prevalent trends (Fig.10). Fractures can be arranged in decreasing order of abundance as follows: NNE-SSW, NE-SW, NNW-SSE and N-S. The ENE-WSW and NW-SE fracture trends are of little effect. So, the studied area is mostly affected by both the gulfs of Aqaba and Suez tectonic trends. These results are agreed with those obtaining by Sharaf (1990) and Sherif (1993). Sharaf (op cit) mentioned that Sinai Peninsula is affected by four fault groups e.g. ENE – WSW, NNW - SSE and NW - SE bound the Gulf of Suez and extend further eastwards into

Sinai and the NNE -SSW that well developed in southern Sinai near the Gulf of Aqaba and extending further northwards and westwards.

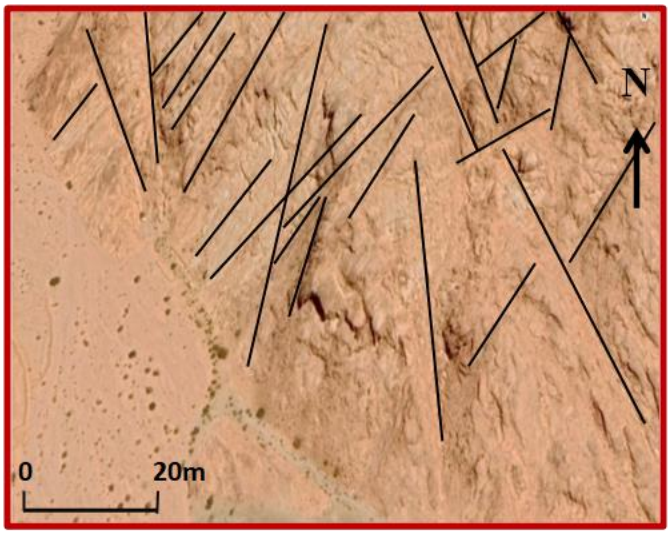

Fig. (8): The anomalies-bearing fractured syenogranite.

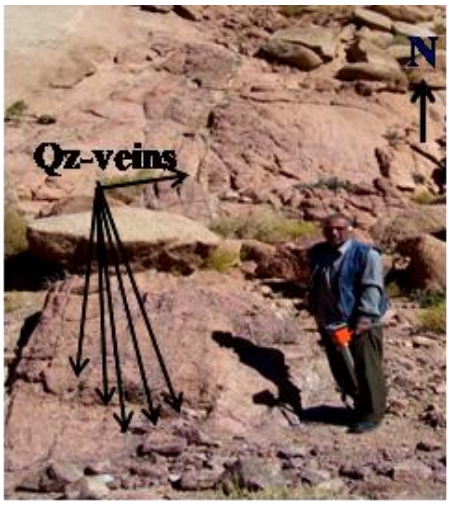

Fig. (9): Highly altered anomalous set of quartz veins in syenogranite.

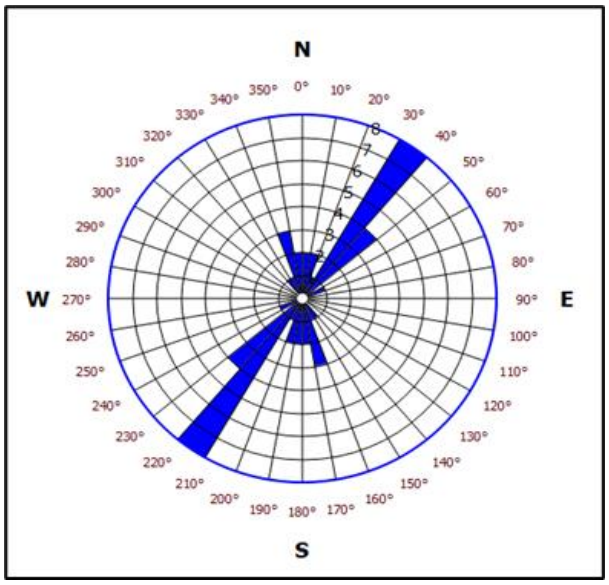

Fig. (10): Rose diagram shows the prevalent fracture trends in the anomalous area.

Table(1): Numbers and intesities of the measured fractures

Facture group	No.	Intensity %
NNE-SSW	7	28
NE-SW	6	24
NNW-SSE	5	20
N-S	4	16
ENE-WSW	2	8
NW-SE	1	4
Total	25	100

3.2. Fluorite-bearing quartz veins:

Veins, in general, are defined as an epigenetic mineral-filling of a fault or other fracture in a host rock in tabular or sheet-like form. Vein-type deposits are dominated in igneous rocks although they occur in both of metamorphic and sedimentary rocks. In igneous rocks, they are closely related to granitic rocks. In the writer's opinion, veins are defined as any ascending or descending fracture-filling materials.

Based on their relation with the granitic rocks, Dahlkamp (1993) classified veins into intragranitic and perigranitic veins. The intragranitic veins are those formed within the granites while the perigranitic type are formed around the granitic plutons. Dahlkamp (op.cit) concluded that the intragranitic vein deposits are commonly monometallic and occur either as (a) linear ore bodies in form of distinct veins or stockworks emplaced in fractured granite or (b) disseminations in pipes or chimneys of

episyenite, a dequartzified, micaceous vuggy alteration product of granite. Depth extension of intragranitic veins is commonly less than 300m.

In the field, however, hydrothermal veins can be recognized by their distinctive white colour and their domination by quartz or calcite. Also, they vary in width from a few millimeters to a meter and are very common in igneous and other terrain.

In the study area, veins occur in parallel form with straight sides and filled with quartz together with deep violet fluorite and occasionally uraninite (Fig.11). Signs of alteration processes are well pronounced along their planes such as hematitization, silicification and kaolinization (Fig.11). The field radiometric studies indicate that the fluorite-bearing quartz veins show high radioelements intensities where eU ranges from 370-780 ppm while eTh content ranges from 340-810ppm (Table 3).The straight sides of these veins may suggest their formation in cold host rocks (Thorpe and Brown,1985).They are usually very much longer than they are wide and vary in thickness. Such type of veins was described by Thorpe and Brown (1985) as hydrothermal veins. The studied veins are classified as intragranitic type according to the classification of Dahlkamp (1993).

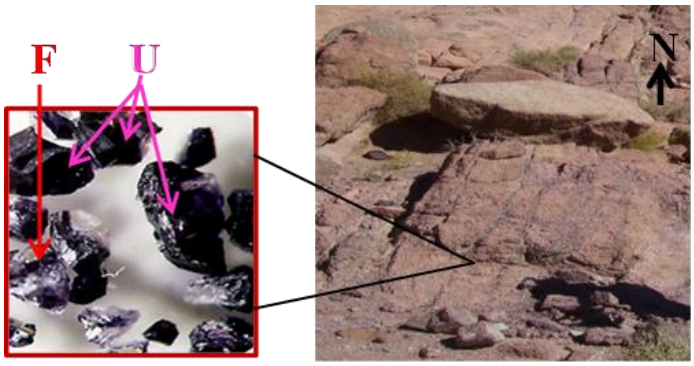

Fig. (11): Alterations along the planes of quartz veins contain uraninite (U) & fluorite (F) mineralizations

4. Spectrometric studies:

4.1 Uranium and thorium distribution in the studied rock units:

The rock units to be radiometrically surveyed are those with acidic nature such as monzogranite, quartz syenite and syenogranite. Because of their low radioactive intensities, the older granites cannot be represented in this study. The measured eU and eTh contents together with their ratios of the studied monzogranite, quartz syenite and syenogranite respectively are presented in table (2). The data obtained are graphically represented (Figs 12, 13 and 14). The two radioelements contained in the studied rock units show scatter distribution due to the effect of the post-magmatic processes. This result is confirmed by the average values of the eU/eTh ratios calculated for the studied rock units (Table 2) which all are exceeding 0.33, i.e. Monzogranite (0.43), quartz-syenite (0.73) and syenogranite (0.74). The 0.33 value for eU/eTh ratio is the ideal magmatic ratio for these two elements. If this ratio is disturbed, post magmatic processes are expected to add or remove uranium.

It is worth to mention that the average values for the eU and eTh of the studied rock units increase from the monzogranite through the quartz-syenite toward the syenogranite (Fig.15). Also, the averages of the eU/ eTh ratios of these rocks follow the same behavior (Fig.16). This conclusion confirms the high concentration of these two elements in the highly differentiated late magmatic intrusion, i.e the syenogranite.

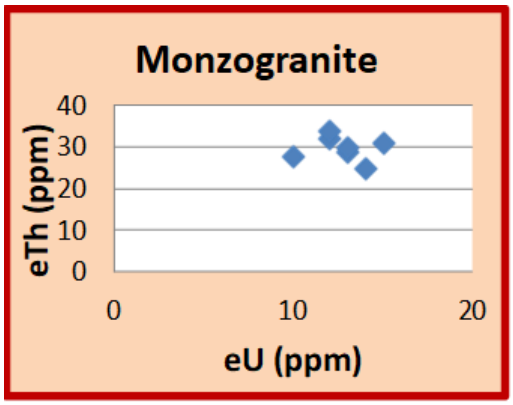

Fig. (12): Plotting of eU VS eTh of the studied monzogranite.

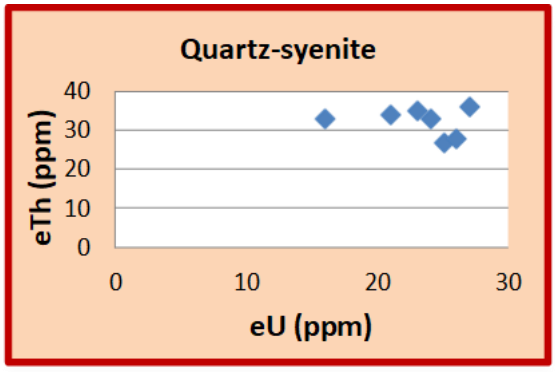

Fig. (13): Plotting of eU VS eTh of the studied quartz-syenite.

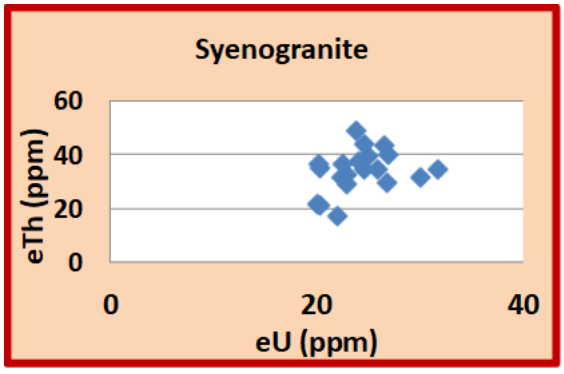

Fig. (14): Plotting of eU VS eTh of the studied syenogranite.

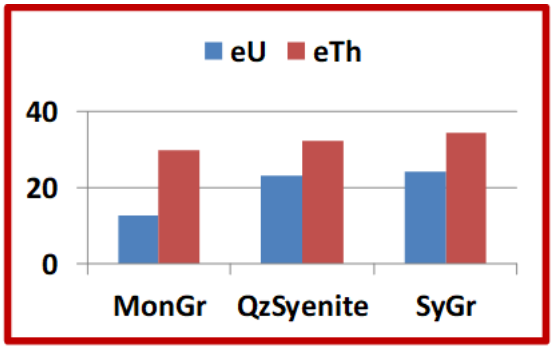

Fig. (15): Plotting of average eU VS average eTh of the studied rock units.

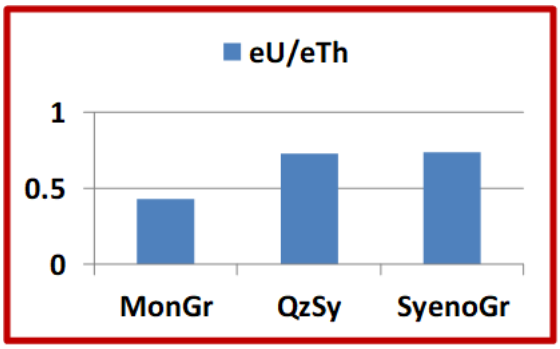

Fig. (16): Plotting of average eU/eTh ratios of the studied rock units.

Table (2): eU (ppm), eTh (ppm) and their ratios in the studied rock units.

Monzogranite						Syenogranite				
	eU	**eTh**	**eTh/eU**	**eU/eTh**		**eU**	**eTh**	**eTh/eU**	**eU/eTh**
	12	32	2.67	0.38		30	31.8	1.06	0.94
	10	28	2.8	0.36		31.7	35	1.10	0.91
	14	25	1.79	0.56		26.7	30	1.12	0.89
Average	15	31	2.07	0.48		22.9	33	1.44	0.69
	13	29	2.24	0.45		26.9	40.3	1.50	0.67
	12	34	2.84	0.35		23.8	49	2.06	0.49
	13	30	2.31	0.43		24.6	35	1.42	0.71
	12.7	**29.9**	**2.38**	**0.43**		24	38	1.58	0.64
Quatrz-syenite						25	39.5	1.58	0.63
	eU	**eTh**	**eTh/eU**	**eU/eTh**	**Average**	25.9	35	1.35	0.74
	25	27	1.08	0.926		22.3	32	1.43	0.69
	26	28	1.08	0.929		22.5	37	1.64	0.61
	16	33	2.06	0.49		20.3	35.3	1.74	0.58
Average	21	34	1.62	0.62		24.5	44	1.79	0.56
	23	35	1.52	0.66		26.5	43.6	1.65	0.61
	27	36	1.33	0.75		20.1	37	1.84	0.54
	24	33	1.38	0.73		22.9	29.2	1.28	0.78
	23.14	**32.29**	**1.44**	**0.73**		20	22	1.10	0.91
						22	17.5	0.80	1.26
						20.3	21.5	1.06	0.94
						24.15	**34.29**	**1.43**	**0.74**

Table (3): ^{40}K%, e U (ppm), e Th (ppm) contents of south Wadi El Barrah area.

S.N	^{40}K%	e U	eTh	S.N	^{40}K%	e U	eTh	S.N	^{40}K%	e U	eTh
1	3.4	27.9	31.6	45	3.2	23.6	32.5	89	3.1	27.3	40.3
2	4.1	31.9	34.7	46	3.1	25.3	29.2	90	3.9	23.5	30.8
3	3.2	26.3	29.2	47	3.7	21.3	29.3	91	3.5	21.2	36.3
4	3.7	22.4	28.4	48	5.1	211	130.3	92	4.1	19.2	22.5
5	4.4	25.1	56	49	4.7	170.	107.5	93	4.6	22.9	31.6
6	3.8	22.4	51.5	50	3.8	111.	59.3	94	4.8	20.6	28.3
7	4.2	24.3	29.8	51	3.2	113	40.3	95	4.8	24.2	28.7
8	3.6	21.7	36.9	52	3.7	97.6	37.9	96	5.8	184.8	98.4
9	3.3	26.6	45.2	53	3.9	54.5	33.8	97	3.9	119.2	79.7
10	2.9	25.4	32.5	54	4.1	23.2	30.6	98	3.4	25.9	46.9
11	3.7	21.3	29.7	55	3.8	21.3	37.5	99	3.7	22.4	37.3
12	4.2	22.8	36.4	56	3.4	23.7	35.5	100	3.9	24.2	35.5
13	3.9	19.3	33.7	57	3.7	24.4	32.9	101	3.5	28.2	38.3
14	3.5	25.4	45.2	58	3.9	21.3	27.7	102	3.9	21.2	28.2
15	3.7	26.1	42.9	59	3.8	25.7	35.7	103	4	23.5	25.3
16	4.1	18.3	35.1	60	5.2	207	126.9	104	4.2	20.2	20.3
17	3.9	19.8	29.8	61	5.1	201	117.3	105	4.5	19.5	28.4
18	3.7	18.8	16.5	62	4.8	95.5	107.8	106	3.9	21.6	26.6
19	4.3	19.3	11.7	63	4.7	38.3	41.3	107	5.1	24.3	34.4
20	3.2	20.6	21.3	64	3.5	27.9	34.4	108	5.3	173.3	69.7
21	3.5	19.7	27.2	65	2.8	28.7	35.6	109	5.6	116.3	67.4
22	3.8	19.1	18.5	66	3.3	29.4	37.6	110	4.1	76.4	82.5
23	3.6	20.7	18.8	67	4.3	26.3	34.2	111	3.7	54.6	74.8
24	2.8	20.4	21.1	68	3.8	27.5	31.3	112	3.2	29.3	43.5
25	3.1	19.3	22.5	69	4.5	26.8	35.5	113	3	27.2	35.1
26	2.9	18.8	21.3	70	4.8	21.7	31.6	114	3.3	23.7	38.9
27	3.4	18.1	19.6	71	3.2	33.4	49.4	115	3.7	19.7	33.2
28	3.6	19.5	23.3	72	5.6	220	126.6	116	4	21.4	37.5
29	3.8	21.2	29.7	73	5.1	196	119.3	117	3.9	26.9	29.8
30	2.7	28.3	33.1	74	4.9	35.3	48.2	118	3.6	23.8	32.7
31	3.6	19.1	21.6	75	3.2	23.3	31.6	119	3.1	25.4	38.3
32	4.5	21.6	22.7	76	3.7	32.4	41.9	120	5.7	125.8	71.7
33	4.6	29.3	31.8	77	3.1	29.9	39.3	121	3.5	119.3	69.6
34	3.1	19.7	25.1	78	3.5	28.3	36.2	122	3.8	30.3	36.7
35	3.4	26.7	34.7	79	3.7	24.4	35.6	123	3.1	27.7	45.3

36	4.9	54.6	90.3	80	3.2	28.9	32.5	124	3.4	24.7	43.5
37	3.4	19.2	16.9	81	2.9	28.4	39.7	125	3.6	25.3	45.2
38	3.6	24.3	37.6	82	3.1	24.6	35.9	126	3	29.3	43.4
39	3.1	23.5	33.5	83	3.4	23.2	34.8	127	4.7	22.6	45.2
40	3.7	24.5	30.5	84	5.3	222	112.8	128	5.3	23.3	34.5
41	3.9	21.9	31.6	85	3.9	1151	87.9	129	5.7	28.5	35.7
42	3.1	23.6	25.3	86	3.3	31.2	55.3	130	5.3	32.3	29.2
43	3.9	26.3	34.2	87	3.6	22.4	41.7	131	3.7	27.5	17.5
44	4	22.3	36.5	88	3.6	29.3	38.6	132	3.6	113.3	69.3

4.2. Spectrometric studies of the anomalous area:

The radioelements distribution of the quartz vein-hosted syenogranites is carried out using multichannel spectrometric instrument model GR-512 for measuring K%, eU and eTh. The measured 132 stations (Table 3) were conducted along twelve equally-spaced profiles, trending at N-S cutting across the strike of the high radioactive zone. The in-between space of each two successive profiles is 15 m with station intervals along any profile is 20m.The odd high radiometric values (Table 4) were excluded to avoid noisy resulted from condensation of contour lines on the obtained radiometric contour maps.

The obtained results will be discussed as follows:

- Figure (17) shows the Potassium distribution contour map where its distribution is dominantly controlled by the NNE-SSW, NE-SW fracture trends and to a lesser extent by N-S trend while the NNW-SSE fracture trend has little effect on its distribution.
- Figures 18 and 19 represent the distribution contour maps for both of eTh and eU respectively. The distribution of eTh is strongly controlled by the NNE-SSW and NE-SW fracture trends and so weakly by NNW-SSE. It is noticed that the distribution of eU is strongly controlled by the NNE-SSW and NE-SW fracture trends while the N-S is less dominant (Fig.11).

Table (4): The excluded values from radiometric map data

S. N.	Long. E	Lat. N	eU	eTh
1	36572055	3183625	780	810
2	36572037	3183604	613	621
3	36572017	3183582	370	340

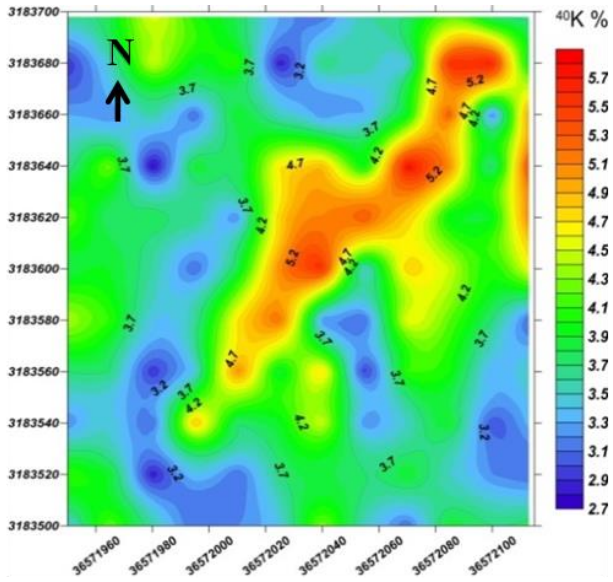

Fig. (17): Potassium distribution contour map.

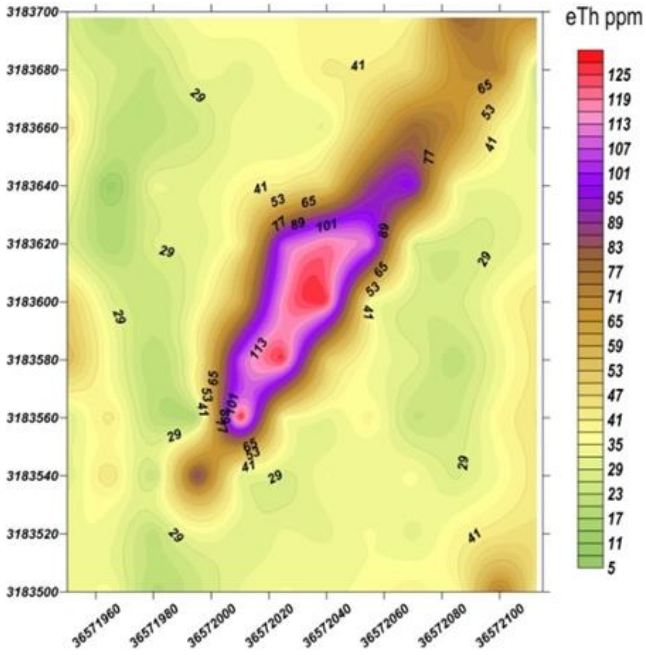

Fig. (18): eTh distribution contour map.

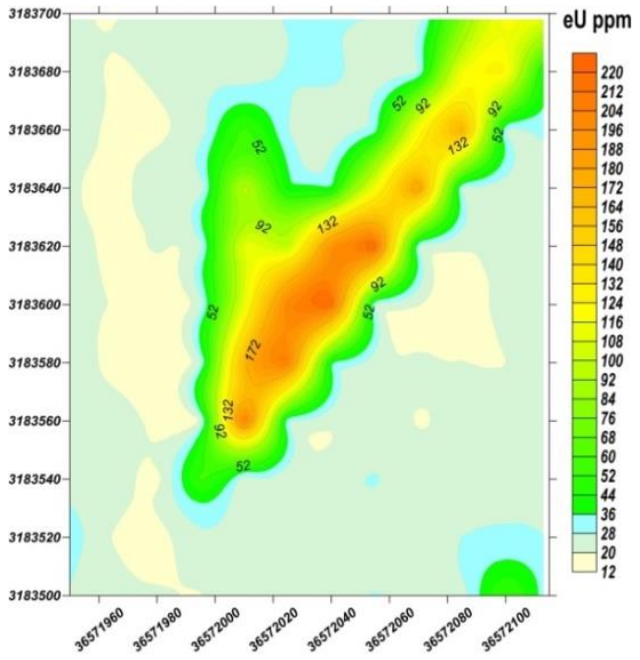

Fig. (19): eU distribution contour map.

5. Mineralogical studies

Five representative radioactive anomalous samples are chosen and treated for mineralogical investigations using both XRD and ESEM techniques where the identified minerals will be discussed in the following paragraphs:

5.1. Uranium and U&Th-bearing minerals.

5.1.1. Uraninite: UO2

Uraninite is a common accessory mineral in pegmatites and peraluminous granites and is the most important source of dissolved uranium in groundwater emanating from weathered granite terrains (Finch, 1996). In the study area, the handpicked uraninite samples taken from the fluorite-bearing quartz veins occur as subhedral black crystals associated with deep violet fluorite (Fig.20A). Both XRD and ESEM investigations of the picked black crystals indicate the presence of uraninite mineral (Fig.20B and C). Figure 20C shows the presence of high ThO_2 content as well as a considerable percentage of FeO, SiO_2 and minor amount of SO_3.

5.1.2. Uranosphaerite: $Bi_2U_2O_9.3H_2O$ $Bi(UO_2)O_2(OH)$ $Bi(UO_2)O_2OH$

Uranosphaerite is hydrated oxide of bismuth and hexavalent uranium, which occurs generally as yellow-orange, reddish-orange, brick-red crystals with spheroid shape. The mineral is considered as an oxidation product of uraninite in a Co-Ni-Bi-bearing hydrothermal vein (Frondel, 1958). Uranospherite and walpurgite are the only known uranium minerals that contain bismuth as a major, essential constituent (Frondel, op.cit). Uranosphaerite is a secondary mineral, formed with various arsenates in the oxidized zone of a vein carrying uraninite, native bismuth, and cobalt-nickel arsenides. UO_3 ranges from 50.88-52.62%, Bi_2O_3 ranges from 42.67 - 44.34% while H_2O 4.95-4.75 %.

In the studied area, uranosphaerite occurs as reddish-orange to brick red anhedral grains associated with black uraninite and hematite (Fig.21). The picked reddish yellow grains are examined using XRD. The data obtained shows the presence of hydrous U and Bi–bearing secondary uranium mineral uranosphaerite (Fig.21).

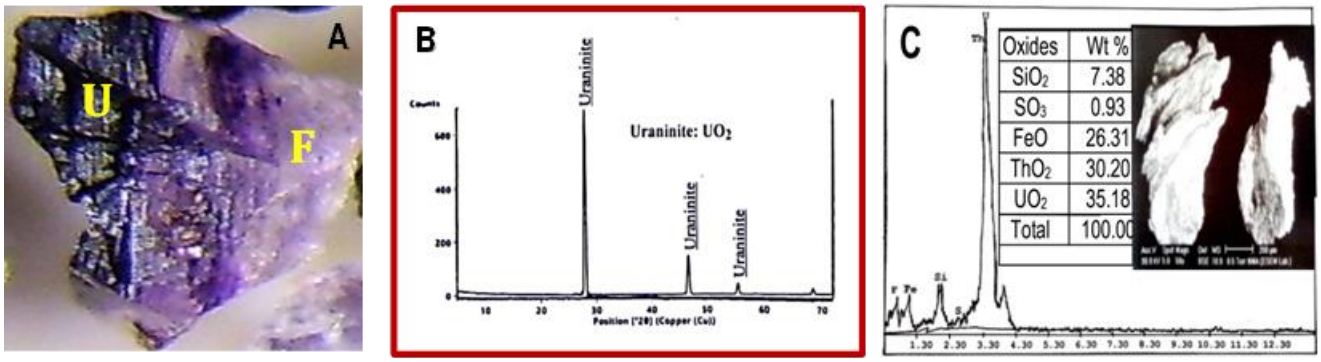

Fig. (20): (A) Photomicrograph shows subhedral black uraninite and deep violet fluorite, (B) XRD pattern of uraninite and (C) BSE images and EDAX of uraninite.

5.1.3. Thorutite: $(Th,U,Ca)Ti_2(O,OH)_6$

Thorutite is a monoclinic-prismatic mineral containing uranium, titanium, thorium, oxygen, hydrogen and calcium. The mineral was named after detection of titanium, thorium and uranium in its composition. Thorutite occurs in syenite massif and veins of microcline and sericitized nepheline. Galena, barite, calcite, zircon and thorite are closely associated with thorutite. Thorutite is widely distributed in Kutyur-Tyube thorium deposit, near Urusai Peak, Sokh River basin, Alai Range, Kyrgyzstan (Gotman and Khapaev, 1958).

In the studied area, thorutite occurs as black anhedral grains. The picked grains are examined using XRD. The data obtained shows the presence of hydrous U,Th and Ti - bearing thorutite mineral (Fig.22). Gotman and Khapaev, (1958) concluded that thorutite is thorium mineral rather

than uranium mineral where ThO_2 = 54.10%, TiO_2= 36.1% while UO_2 and H_2O are relatively low and reach 1.43% and 1.07% respectively.

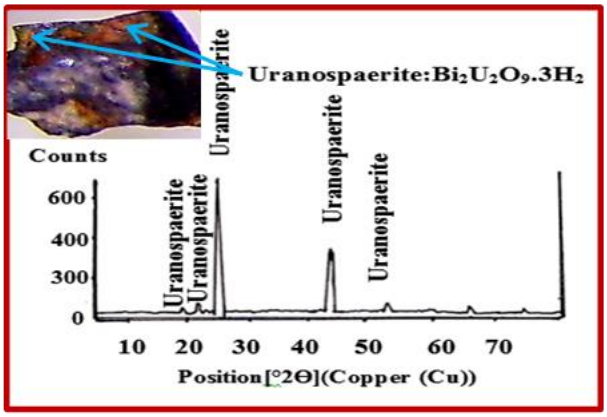

Fig. (21): Photomicrograph and XRD pattern for uranospharite.

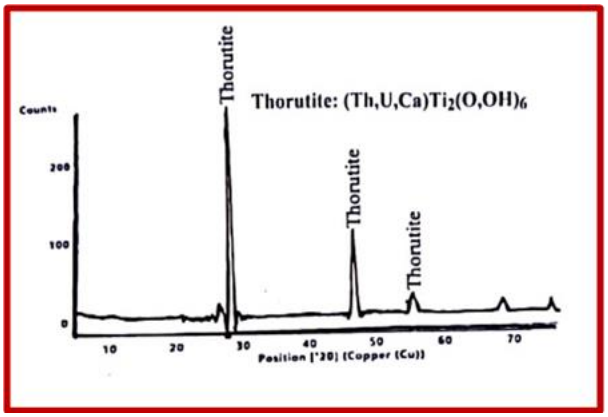

Fig. (22): XRD pattern for thorutite.

5.2. Non-radioactive minerals:

5.2.1. Fluorite: CaF_2:

Fluorite [CaF_2] is a common accessory mineral in many hydrothermal ore deposits, and its dissolution can release F. Fluorite is generally associated with uranium minerals. In the study area, it occurs as white crystals (Fig.23). Sometimes, it occurs as violet to deep violet crystals associated with the uranium minerals in the uraniferous fluorite-bearing quartz veins. The deep violet colour of fluorite is mainly attributed to the radiation effect (Dill and Weber 2010; De Lima and Lameiras 2015). The light violet samples have higher content of calcium relative to fluorine, as well higher content of hydroxyl, probably replacing fluorine in crystal lattice (De Lima and Lameiras, 2015). Consequintly, the deep violet fluorite has higher content of fluorine relative to calcium. The XRD analyses of the deep violet picked grains indicate the presence of fluorite (Fig.23).

5.2.2. Galina: PbS.

Galena is a very common sulphide, the main ore of Pb and often an important ore of Ag. Galina occurs as small black crystals associated with fluorite and uranium mineralization in the studied uraniferous fluorite-bearing quartz vein. The picked black grains are examined using the ESEM technique attached with EDAX unit. The data obtained indicates the presence of galina (Fig.24).

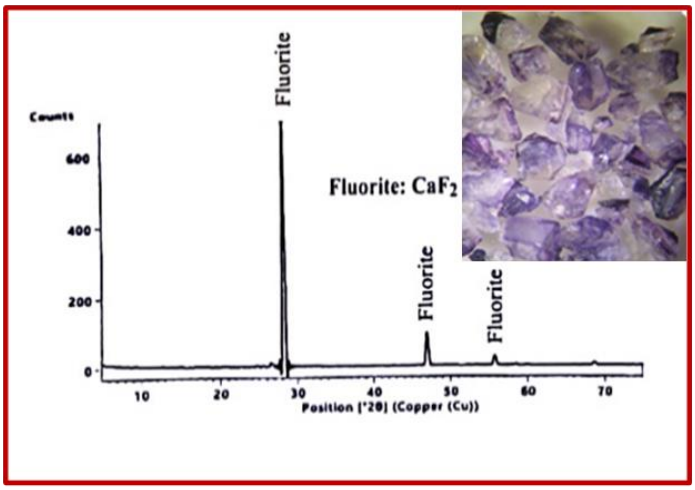

Fig (23): Photomicrograph and XRD pattern of fluorite.

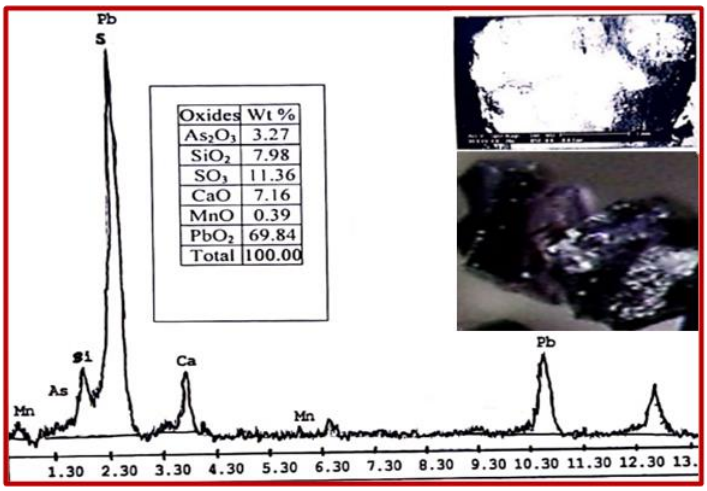

Fig (24): Photomicrograph, BSE image and EDAX of galena.

6. Discussions and conclusion:

General statements:

Uranium is a lithophile element that is enriched in the upper crust by geological processes. Igneous rocks, in general, represent the main source of uranium deposits which form either directly from fluids expelled during crystallization of magmas (primary minerals) or indirectly when alteration and redistribution processes of these primary minerals take place by hydrothermal meteoric solutions (secondary minerals). Generally, uranium and thorium are found to be enriched in the youngest, more

differentiated, more felsic and more potassic members of comagmatic suites of igneous rocks such as two mica granites (Rogers and Adams, 1969).

Behaviour of uranium and thorium in minerals and rocks of igneous origin through magmatic evolution:

The close association of uranium and thorium in both minerals and rocks of igneous origin can be explained based on the crystal chemistry of these elements. During the magmatic cycle, the U-Th coherence is attributed to the more obvious similarities in both their charge and ionic radii; U^{4+} (1.05 A°) and Th^{4+} (1.10 A°). At the "basic" stage of the magmatic evolution, the early formed minerals are olivine and calcic plagioclase. The large and highly charged ions of uranium and thorium cannot inter the lattices of olivine and coordination requirements inhibit the substitution of uranium and thorium in the place of Ca^{2+} (1.06 A°) in plagioclase. Thus uranium and thorium abundances in mafic rocks are low (Aswathanarayna, 1985). At the "intermediate" stage U^{4+} and Th^{4+} could inter into accessory minerals like zircon (Zr^{4+}-0.87 A°) and apatite (proxying for Ca^{2+}-1.06 A°). Thus intermediate rocks, such as diorite and andesite have higher amounts of the two radioelements than the ultramafic and mafic rocks.

At the "acidic" stage, isomorphic substitution of U^{4+} and Th^{4+} and some REE occurs and thus they able to enter into a variety of accessory minerals such as monazite (Ce^{4+}-1.02 A°), allanite apatite, xenotime...etc. All these are characteristic minerals of high temperature environment and usually have Th/U ratios higher than 1, and commonly approaches the crustal ratios of 3.5- 4.

By the progressive of time, the pegmatitic stage is reached, the concentrations of uranium and thorium become sufficiently large to enable the element to form discrete minerals of their own such as samarskite, , monazite, uraninite, etc.

At the hydrothermal stage; U^{4+} and Th^{4+} start losing their geochemical coherence because of the oxidizing environment that characterizes this stage; U^{4+} gets oxidized into highly soluble uranyl ion $(U^{4+}O_2)^{2+}$ and gets more mobile. On the other hand, Th^{4+} is unoxidizable and hence remains behind. This permits, for the first time, the formation of discrete uranium minerals, such as pitchblende.

Mode of occurrence of uranium and thorium in granitic rocks:

In general, the uranium occurred in U-rich granites is considered by Pagel (1982) to be incorporated mainly in accessory minerals, the commonest of which are uraninite, thorite, monazite, xenotime, allanite, zircon, apatite, sphene and Fe-Ti oxides. The author (op.cit) also stated that only a maximum of 20% U is associated with major rock-forming minerals (e.g. plagioclase, orthoclase, hornblende, and biotite. The uranium existing in granites can be genetically divided into two groups: primary uranium and regenerated uranium (Jiashu and Zehong, 1982). The primary uranium can be present in the following forms :

1-Uranium minerals occur as accessory minerals in granite such as uraninite, uranothorite and brannerite.

2-Uraniferous minerals contain less than 5% uranium such as thorite, thorianite pyrochlore, betafite, samarskite, euxenite polycrase, allanite, sphene, monazite, xenotime, zircon, etc .

3-Submicroscopic uraniferous particles which occur as extremely tiny particles non-homogenously distributed in the crystals of the rock-forming minerals.

4- Homogenously scattered uranium atoms which are most probably homogenously scattered in rock-forming minerals, making up part of the background content of uranium.

In these granites, uranium and thorium may also accumulate along the intergranular boundaries and fractures or they may be entrapped in lattice imperfections or adsorbed on the surface of crystal faces. Thus it is estimated that about 40% of uranium contained in the granites is not fixed in crystal lattice of minerals and so it is readily leachable with dilute acids (Sherif,1998).

Fracture analyses:

Sinai Peninsula was affected by various tectonic events that resulted in the formation of several faults that have different intensities and trends such as NNE-SSW, NE-SW, NNW-SSE, N-S, ENE-WSW and NW-SE (Abd El Gawwad, 1969;Meshref,1971;Abu El-Ata, 1988; Rabie and Ammar,1988).

The NNE-SSW, N-S, NW-SE and NE-SW fractures are predominant trends for uranium mineralization in the eastern desert of Egypt and south Sinai. In south Sinai, several types of uranium mineralizations are recorded along numerous shear zones, pegmatites and quartz veins having the above mentioned trends **[**(El-Regeita, Um Zariq and Ghazala areas, Bishr, 2003 and Bishr et al 2009); (Um Alawi, El-Rusis, Wadi Akhdar areas, El Akeed, 2009 and 2014); (Wadi Zaghra area, Sallam et al, 2019); (Wadi Seih area, Sherif ,1998); (Wadi El Barrah area, Sherif, 1993; El Galy, 1994 and Gabr, 2005); (Wadi Sahu area, Bishr ,2003 and Gabr 2005)]

Although some of secondary uranium minerals such as kasolite and uranophane are recoded by Sherif (1993) El Galy (1994) and Gabr (2005) in the NNE-SSW and NE-SW trending fluorite-bearing quartz veins in the studied syenogranites, uraninite is firstly recorded in these veins at this study.

In the eastern desert of Egypt, primary and secondary uranium mineralizations are recorded in jasparoid vein associated with NW-SE, NE-SW and ENE-WSW trending shear zones in El-Missikat area (Ibrahim, 2002; Abu Deif and El Taher,2008). Ibrahim et al. (2001) studied the uranium mineralization in the two mica granites of Gabal Ribdab area, South Eastern Desert and found that they are localized along the N-S and NNE-SSW fractures trends. Also, the uranium mineralizations of El Sela granite are generally localized along the E-W to ENE-WSW striking shear zone and N-S to NNE-SSW set of fault (Gaafar et. al. 2014). Moreover, the uranium mineralizations of Gabal Gattar granites are controlled mainly NNE-SSW, ENE-

WSW, NW-SE and to a lesser extent the N-S trending faults (Roz,1994; Salman et al 1994; Salman et al. 1996 and Waheeb, 2017).

In the present study, there are numerous fluorite-bearing quartz veins and fractures having NNE-SSW, NE-SW, NNW-SSE and N-S trends (Figs.8,9, and 10). These veins and fractures are cutting through the studied syenogranites and having anomalous radioactivity where eU ranges from 370ppm to 780ppm while eTh ranges from 340ppm to 810ppm (Table 4). The high eU content is due to the presence of uraninite and uranosphaerite minerals while high eTh content is due to the presence of Th-bearing mineral thorutite.

Origin of uranium and thorium mineralizations:

The studied area is covered with igneous rock suite comprising older granites, monzogranite, quartz syenite and syenogranite. The eU and eTh contents are gradually increased from the monzogranite through quartz syenite to be higher at the syenogranite (Table 2), i.e. increased with magma evolution. The studied syenogranite is composed mainly of quartz, potash feldspars, plagioclase along with biotite and subordinate muscovite as well as zircon, fluorite, apatite and iron oxides (Sherif, 1993; El Galy, 1994; and Hussein et al, 1999). It also has more than 75% SiO_2 and derived from peraluminous magma (Ibrahim and Khalifa, 2004; Sherif, 1993; and Hussein et al, 1999). Accordingly, the studied syenogranite is considered as more acidic, highly differentiated, peraluminous two-mica granite which is more favored for incorporating of both uranium and U-bearing minerals. The studied syenogranite is considered as uraniferous and fertile granite where it contains 24.9 ppm eU (Table 2) more than twice the Clarke value for uranium. The uranium presents in this syenogranite is easily leached by hydrothermal solutions that percolated through the developed brittle fractures (Fig.8) and transported to be finally precipitated in any favorable environments.

The U fertility of granites not only depends on their total U content but also on the capacity of the U-bearing phases they host to be dissolved by the fluids. In peraluminous leucogranites, uranium is mainly hosted as uranium oxides and, as such, represents an ideal source for the formation of U deposits (Gaafar et al., 2014) as uranium oxide is an extremely unstable mineral and consequently easily leachable during oxidizing fluid circulations.

The resultant hydrothermal solutions, which are originally rich in silica, can dissolve uranium and probably other elements. Uranium is generally transported as uranyl ion $(UO_2)^{2+}$ by the silica-rich hydrothermal solutions together with dissolved other elements. These solutions are ascending through the fractures developed in the studied syenogranite and finally cooled to precipitate U-bearing quartz veins. In this case, uranium is precipitated in its hexavalent state. A period of an oxygen deficiency and hence low oxygen fugacity is prevailed in quartz veins's environment indicated by the presence of ferrous iron and sulfur (Fig.21). Accordingly, the hexavalent uranium can be reduced to be tetravalent uranium and hence uraninite can be formed. Hexavalent uranium may also be effectively reduced by a mechanically induced decrease in the oxygen fugacity of the system as the temperature, pressure, and pH of the hydrothermal fluid changes with upward migration into and through dilatant zones (Mathews and Pilcher, cited in Mickle and Mathews, 1979).

As is recognized by many investigators, in hydrothermal solutions bivalent iron, sulfide sulfur, and organic matter may be precipitants of hexavalent uranium with the formation of uranium oxides. This opinion is supported by experimental investigations of Rafal'skii (1958) who paid a particular attention to iron as a reducer of hexavalent uranium because in many uranium deposits hematization of the adjoining rocks is observed, as a result of which the latter acquire a red color of varying shade. He also stated that the Fe-bearing mafic minerals - both vein minerals and those of the rocks adjoining the uranium mineralization may be a source of bivalent iron. The reduction of uranium by iron may be represented as follows:

$U^{6+} + Fe^{2+} \rightarrow U^{4+}$ (uranium oxides) + F^{3+} (hematite). In the case of transfer of uranium in the tetravalent form, its precipitation from hydrothermal solutions as oxides is explained primarily by the change in the pH of the solutions as a result of their reaction with the adjoining rocks.

The high ThO_2 content presents in the studied uraninite (30.20%, Fig.20) requires an abundance of fluorine in the fluid phase to transport sufficient amounts of Th (Moin et al., 1998). The presence of fluorine is indicated by the presence of its own mineral fluorite (Fig.23). The high ThO_2 content presents in the studied uraninite may also attributed to the presence of some Th-bearing inclusions such as thurotite.

Another subsequent widespread phase of thermal activity is occurred contemporaneous with the intrusion of the post-syenogranite dyke swarm in the studied area. This can be expressed by the alteration products that developed in both host rocks and along the quartz veins such as hematitization, kaolinization and silicification (Fig.11). This phase can cause marginal alteration of the uraninite and produce the recorded secondary uranium mineral uranosphaerite (Fig. 21).

The association of fluorite (Fig. 23) and galena (Fig. 24) with uranium minerals present in the studied quartz veins suggest the hydrothermal origin of these veins.

References

Abd El Azeem, A. A. (2019): Geological And Radioactivity Studies On The Dykes Of Wadi El Akhdar Area, Southern Sinai, Egypt. Nuclear Sciences Scientific Journal 8, 181- 202

Abd El Gwad, M. (1969): New Evidences of transcurent movements in Red Sea area and Petroleum Implications. Am. Assoc. Petrol. Geol. Bull., V.53, No7, 1466-1479.

Abu Deif, A. and El-Tahir, M. (2008): A New Uranium Occurrence, Gabal El-Missikat Prospect, Central Eastern Desert, Egypt. JKAU: Earth Sci., Vol. 19, 85-97.

Abu El Ata, A. .S. .A. (1988): The relation between the local tectonics of Egypt and the plate tectonics of the surrounding

regions, using geophysical and geological data. E.G.S. Proc.of the 6th Ann. M., March, 92-112.

Abu El-Lei, I. (1980): Geology, petrography and geochemistry of some granitic rocks in the northern part of the basement complex. Egypt. Ph.D. thesis, Al- Azhar Univ. Cairo. Egypt. 270 pp.

Akaad, M. K. and El Ramly, M. F. (1960): The Basement Complex in the South-Central Eastern Desert of Egypt between Latitudes 25°00'N and 25°30'N, Geological Survey of Egypt (Paper 8, 35 p). Costa Tsoumas, Printers.

Akaad, M. K., Noweir, A. M. and Kotb, H. (1979): Geology and petrochemistry of the granite association of the Arabian Desert Orogenic Belt of Egypt between Lat. 25° 350 and 26°300. Delta Journal of Science. 1979;3: 107-151

Akaad, M. K. and Noweir, A. M. (1980): Geology and lithostratigraphy of the Arabian Desert Orogenic Belt between latitudes 25° 35` and 26° 30` N. Symp. on "Evolution and Mineralization of Arabian and Nubian Shield". Inst. Appl. Geol. (Jeddah), Bull. 4(3): 127-135.

Aswathanarayna, U. (1985): Principles of nuclear geology. Oxonian Press, Sauger University, Sagar, 88–90

Bentor, Y. K. (1985): The crustal evolution of the Arabo-Nubian Massif with special reference to Sinai Peninsula. Precambrian Res. 28, 1–74.

Bishr, A. H. (2003): Geology, radioactivity and mineralogical studies of some granitic plutons in Wadi Um Hamd environs southwestern Sinai, Egypt. M. Sc. Thesis, Mansoura Univ., Egypt. 132 p.

Bishr, A., Azzaz, S., Sherif, H. and El- Aassy, I. (2009): Primary uranium mineralizations in sheared pegmatite of wadi El-Regeita area, south Sinai, Egypt. Delta J. Sci. 32: 32-47.

Dahlkamp, F. (1993): Uranium ore deposits. Originally published by Springer-Verlag Berlin Heidelberg New York in 1993.

De Lima, G. M. and Lameiras, F. S. (2015): COLOR CHANGE OF GEMSTONES BY EXPOSURE TO GAMMA RAYS. 2015 International Nuclear Atlantic Conference - INAC 2015 São Paulo, SP, Brazil, October 4-9, 2015 Giovanna L. C. de Lima1 and Fernando S. Lameiras2.

Dill, H. G. and Weber, B. (2010): Variation of color, structure and morphology of fluorite and the origin of the hydrothermal F-Ba deposits at Nabburg-Wölsendorf, SE Germany. April 2010Neues Jahrbuch für Mineralogie - Abhandlungen 187(2):113-132.

El Akeed, I. A. (2009): Geology and potentiality of uranium in granite and associated rocks in Saint Katherine area, south Sinai, Egypt. Ph.D. thesis, Mansoura University, Faculty of Science (Dameitta). 287p.

El Akeed, I. A. (2014): Uranium Mineralization and Rare Metals Associating Shear Zone in the Younger Granites at Wadi Akhdar Area, Southwestern Sinai, Egypt. Egy. J. Pure & Appl. Sci. 2014; 52(2):7-23

El Galy, M. M. (1994): Geochemical and radiometfic studies of some granitic rocks at Gabal Hamra area, Southwestern Sinai, Egypt. M. Sc. Thesis, Tanta Univ. Egypt, 200p.

El Gammal, S. .A. .S. (1986): Geology of the granitoid rocks of the northwest part of the basement rocks in Sinai, Egypt. Ph.D. Thesis, El Azhar Univ. Cairo, Egypt. 252p

El Sayed, A. .A., Mansour, M. G., Sherif, H. M. and El-Mowafy, A. .A. (2004): Radiometry And Alpha- Track Analyses Of The Stream Sediments Of Wadi Iqna, South Sinai, Egypt. Proceeding of the 7th Conf. Geology of Sinai for Development Ismailia, 2004, 403-411

El Sheshtawy, Y. .A. (1984): Petrographical and geochemical studies of the granitic rocks around Wadi El Sheikh, southwest Sinai, Egypt. Ph.D. Thesis, El Azhar Univ. Cairo, Egypt. 213p.

Finch, W. I. (1996): Uranium provinces of North America – Their definition, distribution, and models. U. S. G. S. Bull., 2141 p.

Frondel, C. (1958): Systematic mineralogy of uranium and thorium. U.S. Geol. Sur. Bull. 1064, 98-99

Gaafar, 1., Cuney, M. and Abdel Gawad, A. (2014): Mineral Chemistry of Two-Mica Granite Rare Metals: Impact of Geophysics on the Distribution of Uranium Mineralization at El Sela Shear Zone, Egypt. Open Journal of Geology, 2014, 4, 137-160

Gabr, M. M. (2005): Zircon typology and uranium mineralization of some younger granite plutons, south western Sinai, Egypt. Ph. D. Thesis, Suez Canal Univ. Egypt. 156 p.

Gotman, Y. D. and Khapaev, I. A. (1958): Thorutite – a new mineral of the group of titanites of thorium. Zap. Vses. Mineral. Obshch., 87, 201–202 (in Russian).

Habeeb, A. .N. (1989): Geology of some granitic rocks from south Sinai, Egypt. M.Sc. Thesis, Zagazig Univ., Egypt. 163p.

Hussein, A. A., Ali, M. M. and El-Ramly, M. F. (1982): A proposed new classification of the granites of Egypt. J. Volc. Geoth. Res., 14: 187-198.

Hussien, H. A., El Shazly, A. G., El Aassy, I. E. And El Galy, M. M. (1999): Petrogenesis Of Pan-African Granitoids, Gabal Hamra Area, Southwestern Sinai, Egypt. A. K. Sinha (ed.), Basement Tectonics 13, 119-138.

Ibrahim, S. K. and Khalifa, I. H. (2004): Geochemistry and petrogenesis of the granitoid rocks at Wadi Barah- Wadi Sahab area, south Sinai, Egypt. Al-Azhar Bull. Sci. 2004; 15: 1(June): 151- 168.

Ibrahim, M. E., Saleh, G. M. and Abd El-Naby, H. H. (2001): Uranium mineralization in the two mica granite of Gabal Ribdab area, South Eastern Desert, Egypt. Applied Radiation and Isotopes 55 (2001) 861–872

Ibrahim, T. M. (2002): Geology and radioactivity studies of the basement sedimentary contact in the area west Gabal El Missikat, eastern Desert of Egypt. Ph.D. theses, Mansoura Univ. Mansoura, Egypt.213p.

Jiashu, R. and Zehong, H. (1982): Forms of uranium occurrence and its distribution in uraniferous granites. In: Geology of granites and their Metallogenetic Relations. Sviences Press, Beijing. 621-635.

Meshref, W. M. (1971): The application of magnetic trend analysis to the interpretation of Egyptian tectonics. 9th An. Mg. Geol. Soc. Egypt., 14-21.

Mickle, D. G. and Mathews, G. M. (1979): Geologic Characteristics Of Environments Favorable For Uranium Deposits. Prepared For The U.S. Department Of Energy Grand Junction Office Under Contract No. Ey-76-C-13-1664.

Moine, B., Ramambazafy, A., Rakotondrazafy , M., Ravolomiandrinarivo, B., Cuney , M. and de Parseval, P. (1988): The role of fluor-rich fluids in the formation of the thorianite and sapphire deposits from SE Madagascar. Goldschmidt Conference Toulouse 1998.

Pagel, M. (1982): Successions paragenetiques et teneurs en uranium des mineraux accessories dans les roches granitques: guides pour la recherche de granites favorables a la presence de gisements d'uranium. Compres-rendus du Symp. "Methods de prospection de l'uranium", Paris, OCDE edit, 445-456.

Rabie, S. I. and Ammar, A. .A. (1988): Maximum principal stress and tectonic trends as revealed from aeromagnetic and aeroradiometric data, Gabal Maghrabia area, Eastern Desert, Egypt. J. Geol.,32,1-2,91-129.

Rafal'skii, R. P. (1958): "Experimental investigations of the conditions of transfer and deposition of uranium by hydrothermal solutions," Report No. 2067, presented to the Second International Conference on the Peaceful Use of Atomic Energy (Geneva, 1958).

Rogers, J. J. W. and Adams, J. A. S. (1969) Uranium and Thorium, In: Wedepohl, K.H., Ed., Handbook of Geochemistry , Vol. 113, Springer, Berlin, 92-B-1 to 92-0-8 and 90-Bb-1 to 90-00-5.

Roz, M. E. (1994): Geology and Uranium Mineralization of Gabal Gattar Area, North Eastern Desert, Egypt. Unpublished M.Sc. Thesis, Al Azhar University, Cairo, 175 p.

Sabet, A. H., Bessoneko, V. V. and Bykov, B. .A. (1976): The intrusive complexes of the central Eastern Desert of Egypt. Ann. Geol. Surv. Egypt.,8,53-73.

Sallam, O., Al Shami, A. and Abbas, A. (2019): Geology And Mineralogy Of A Radioactive Pegmatite Body At Wadi Zaghra Area, Southeastern Sinai, Egypt. Nuclear Sciences Scientific Journal 8A, 191- 205

Salman, A., Shalaby, M., Noseir, L., El Khouly, D., Roz, M., Abu Zeid, M., Mostafa, M., Ayoub, R. and Khamis, H. (1994): Gebel Gattar Prospect, an Obvious Model of Intragranitic Uranium Mineralization. Second Arab Conference on the Peaceful Uses of Atomic Energy, Cairo 5-9 Nov. 1994

Salman, A. B., Shalaby, M. H., Ragab, A. and Abu Zaid, M. M., (1996): Relation Between Uranium Mineralization and Structural Features, Gebel Gattar, North Eastern Desert, Egypt. Third Arab Conference on the Peaceful Uses of Atomic Energy, Damascus 9-13 Dec. 1996 AAEA

Sharaf, M. (1990): Basement Tectonic And Depocenters Distribution In Sinai Peninsula, Egypt. Sci. J. Fac. Menoufia Univ. Vol. IV (1990). 205 -224

Sherif, H. M. Y. (1998): Geology and Uranium potentiality of Wadi Seih area, southwestern Sinai, Egypt. Ph.D. Thesis, Cairo Univ. Fac. of Sci., Geo. Depart. 1998.

Sherif, H. M. (2003): Primary uranium mineralization of Wadi El-Beida granite pegmatite, south Sinai, Egypt. Egypt. J. Geol., 47/1, pp. 175-188.

Sherif, H. M. (1993): Geology and radioactivity studies of Wadi El Berra area, South Sinai, Egypt. M. Sc. Thesis, Suez Canal Univ., Egypt.

Sherif, H. M., El Akeed, I. A., Gabr, M. M. and Naser, M. M. (2022): Mineralogical Studies And Radioactivity Of Wadi Steih Stream Sediments, South Sinai, Egypt. Al-Azhar Bulletin of Science, Section D, Vol. 33, No. 1 (June) 2022, pp. 179-196.

Stratigraphic Chart 2022" (PDF). International Stratigraphic Commission. February 2022. Retrieved 22 April 2022.

Thrope, R. S. and Brown, G. C. (1985): The field description of igneous rocks. Open University Press. Great Britain. P. 151.

Waheeb, A. (2017): Detailed Structural Analysis For The Mineralized Shear Zones of g-Ii uranium Occurrence At Gabal Gattar Younger Granite Northern Eastern Desert Egypt. International Journal of Innovations in Engineering and Technology (IJIET)